Effect of Microdomain Structure and Process Conditions on the Mechanical Behavior of Cylindrical Block Copolymer Systems

Mohit Mamodia, Ashoutosh Panday, Samuel P. Gido, and Alan J. Lesser*

Department of Polymer Science and Engineering, University of Massachusetts, Amherst, Massachusetts 01003

Received January 2, 2007; Revised Manuscript Received July 12, 2007

ABSTRACT: We investigate the effect that process conditions have on the structural characteristics and mechanical response of a cylindrically phase-separated poly(styrene−ethylene-*co*-butylene−styrene) (SEBS) triblock copolymer system. Small-angle X-ray diffraction (SAXD) and transmission electron microscopy (TEM) have been used to study the microdomain and grain structure, respectively. It is observed that the structural changes that occur with different process conditions and thermal treatment alter the mechanical behavior in both monotonic tensile and cyclic tests. Results show that the *d*-spacing decreases with increasing temperature and increasing cooling rate from the melt state. These subtle changes in *d*-spacing are correlated with the elastic modulus. Such variations in domain spacing and size depend on the segregation power (χ) of the system. Grain size changes significantly with cooling rate and upon annealing fine-grain structures but has no significant effect on the material's modulus.

1. Introduction

A common class of thermoplastic elastomers (TPE) includes block copolymers that are covalently joined homopolymer chains. These materials undergo phase separation upon cooling to form ordered lattices such as spheres, cylinders, and lamellae at nanometer scales. At a microscopic scale, the cylindrical and lamellar systems form individual grains with accompanying grain boundaries. Cylindrical and lamellar block copolymers develop a structural hierarchy because they nucleate and grow ordered domains randomly as the material is cooled. Because of their unique morphological and mechanical behavior, studies of TPEs are quite important for fundamental and practical knowledge. Most studies[1−4] on thermoplastic elastomers have focused on characterizing their morphology and phase behavior. Thomas and co-workers[5] investigated the tensile behavior in oriented single-grain lamellar and cylindrical structures. However, relatively few studies[5−9] have focused on what effect, if any, the structural characteristics such as grain size and grain boundaries have on the mechanical response of a polygrain structure.

The grain structure forms through a complex interplay between thermodynamic and kinetic factors. Hashimoto and co-workers have shown that annealing highly asymmetric block copolymers increases their grain size, resulting in a commensurate decrease in the grain-boundary area as well as perfecting the order within the grain.[10] The grain size was also found to depend on the quench depth in quiescently cooled systems.[11] Gido and co-workers used transmission electron microscopy (TEM) to characterize and model the local morphology and grain boundaries in lamellar-based systems.[12−14] Attempts have also been made to measure the grain size of block copolymers by various techniques including polarized light scattering, birefringence, and electron microscopy.[15−20] Yet, how these structural characteristics control the mechanical behavior has not been reported. Further, lamellar block copolymer systems have been used in most of these studies because they are relatively easy to characterize. However, cylindrical block copolymer systems have more commercial relevance, since they exhibit the best overall elastomeric behavior.

Earlier work by Indukuri and Lesser[21] utilized small-angle X-ray diffraction (SAXD) and wide-angle X-ray diffraction (WAXD) to evaluate and correlate structural changes to various amounts of strain in cylindrically phase-separated systems. Their studies show that cooperative microbuckling occurs in these systems and is responsible for the Mullins effect observed in these systems. This buckling instability is expected to depend on the modulus and diameter, but further studies are necessary to confirm this.

In some TPEs the resulting phase morphology can be altered with process conditions and thermal history. Hashimoto[22] and Balsara[23] showed that order-to-order transition (OOT) and order-to-disorder transition (ODT) are profoundly influenced by sample preparation and thermal history. Process conditions and temperature also have an effect on the *d*-spacing of block copolymers.[10,24,25] The *d*-spacing is related to the distance between cylindrical domains as well as cylinder diameter.[26] In block copolymer systems showing an ODT with increasing temperature, it was observed that the *d*-spacing scales as $d \sim T^{-1/3}$, where T is absolute temperature. This effect is attributed to the change in interaction parameter (χ) (i.e., χ decreases with increase in temperature). However, what effect these subtle changes in microstructure have on the resulting mechanical behavior is not known.

In this paper, we present results from systematic studies aimed at identifying what structural parameters in cylindrically phase-separated systems govern their elastic response. Herein we correlate characteristic structural parameters to changes in elastic modulus. The effects of process conditions and thermal treatment are also investigated and discussed in terms of both structural characteristics and mechanical response.

2. Experimental Section

2.1. Materials and Sample Preparation. The material used in this study is a poly(styrene−ethylene-*co*-butylene−styrene) (SEBS) triblock copolymer provided by Kraton polymers, US LLC. The chemical structure of the SEBS triblock copolymer is shown in Figure 1. The number-average molecular weight, M_n, as determined by GPC is 107K g/mol, and the polydispersity index, M_w/M_n, is

* To whom correspondence should be addressed. E-mail: ajl@polysci.umass.edu.

10.1021/ma070006+ CCC: $37.00
Published on Web 09/05/2007

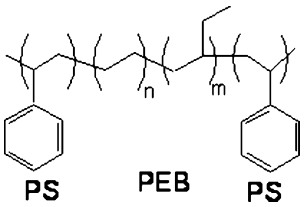

Figure 1. Chemical structure of SEBS triblock copolymer.

1.14 with M_w being the weight-average molecular weight. The weight fraction of PS for this triblock copolymer is 18−22% and contains 0.06−0.14 wt % of antioxidant.

Samples for mechanical and morphological characterization were prepared by three different methods. The first method involved melt processing of thick films using a PHI-PW225C bench press. The material was heated to a temperature well above the ODT temperature (210−220 °C)[27] and below the degradation temperature (350 °C). The samples were maintained at a temperature of 250−260 °C and a pressure of 950 kPa for 30 min and then cooled at different rates, which will be discussed in detail later.

A second method involved solution-casting films. The block copolymer was first dissolved in a nonpreferential solvent (i.e., toluene) to obtain a 5 wt % by volume solution. Solvent evaporation then occurred over a period of 8−10 days at room temperature. The films were then dried at 45 °C for 6 h to remove the excess solvent. Some of these films were characterized without further heat treatment, while others were subjected to different annealing temperatures and times followed by a quench in an ice water bath.

A third method involved extruding samples in a C.W. Brabender single-screw extruder with a screw of $^3/_4$ in. diameter and length-to-diameter ratio of 25:1. The extruder has four zones along the screw where the temperature can be controlled. A constant temperature was maintained throughout the length of the screw for two samples extruded at 170 and 190 °C. A higher temperature ($T \sim 190$ °C) near the hopper (zone 1) and a temperature of 165 °C at the opening of extruder were maintained for one of the sample.

2.2. Characterization and Testing. *2.2.1. Morphological Characterization.* Sections with a 40−50 nm thickness were obtained by cryo-microtoming the bulk films using a Leiica EM-FCS microtome at −90 °C. These sections were then collected and stained with ruthenium tetroxide (RuO_4) for ∼20 min. TEM was performed using a JEOL 100 CX TEM operating at 100 kV.

SAXD measurements were performed on a Molecular Metrology SAXD instrument with a sealed-tube source. Cu Kα radiation with a wavelength of 0.154 nm was used. A three-pinhole collimation system produced a spot size at sample of 700 μm. The raw data were calibrated for the peak position with the standard silver behenate, which has peak position at scattering vector, $q = 1.076$ nm^{-1}. The sample-to-detector distance was found to be ∼1.2 m using the above calibration. Each profile was recorded at room temperature over a period of 1 h, unless a different temperature (or time) is mentioned. The intensity of the scattered beam is taken directly without any background subtraction. The profiles are represented as a function of magnitude of scattering vector, q, which is related to the scattering angle, θ. The Braggs d-spacing in cylindrical block copolymer systems corresponds to the spacing between (100) planes in hexagonally packed PS cylindrical domains.

2.2.2. Mechanical Testing and Thermal Analysis. Monotonic tensile and cyclic tests were performed on an Instron 5800 tensile testing machine. All the tests were performed on ASTM D1708 test geometry (gauge length = 22 mm). All the tests (monotonic tensile and cyclic) were performed at room temperature at a cross-head speed of 10 mm/min. Thermogravimetric analysis (TGA) was done on TGA2950 thermogravimetric analyzer (TA Instruments) on 7.97 mg of sample at a heating rate of 10 °C/min to measure the degradation temperature of the block copolymer. Differential scanning calorimetry (DSC) was performed on a TA Instruments DSC Q1000 at a scan rate of 5 °C/min.

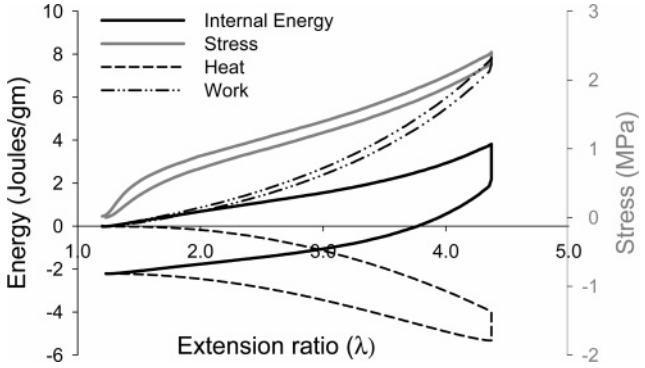

Figure 2. Energetics of deformation of the cylindrical block copolymer.

2.2.3. Deformation Calorimetry. Deformation calorimetry was performed to investigate whether any strain-induced crystallization develops in this system. The incremental work done (dW), heat absorbed (dQ), and hence the internal energy changes (dU) are measured during deformation as described previously.[21,28,29] The calorimeter has been used to study the heat and internal energy changes in strain-crystallizing natural rubber[30,31] and thermoplastic elastomers.[29] The test in this study was performed on ASTM D1708 test geometry at a strain rate of 1.08 mm/mm/min and at a temperature of ∼25 °C.

3. Results and Discussion

3.1. Deformation Calorimetry. In order to investigate whether the composition used in this study undergoes strain-induced crystallization, deformation calorimetry was conducted. A melt-processed sample was used for this test. Figure 2 is a plot of the work done (ΔW), heat released (ΔQ), the change in internal energy (ΔU), and the true stress (σ) all as a function of strain. Note that ΔU remains positive while loading the sample. This indicates that this material does not undergo strain-induced crystallization. Different compositions in different studies[29,30] have been shown to cause strain-induced crystallization, and the extent of crystallization was measured by negative changes in ΔU. However, this does not occur in this system. DSC studies indicate an absence of melting endotherm or crystallization exotherm in heating and cooling scans, respectively. Therefore, this material lacks the ability to crystallize thermally as well.

3.2. Melt-Processed Films: Effect of Cooling Rate. Melt-processed samples were heated above the ODT (∼210−220 °C for this material[27]) and then cooled to room temperature at four different rates. The times taken to cool these samples from disordered state to room temperature were less than 1 min (quenched), 5−6 min (fast cool), ∼90 min (medium cool), and 6−7 h (slow cool). TEM images (Figure 3) reveal a significant difference in the grain size for these systems. As expected, the grain size is largest for the slow-cool system and decreases with increasing cooling rate. In the case of the medium-cool system, the grain size is between that of fast-cool and slow-cool systems, while the quenched system shows a wormlike structure.

Figure 4 compares the SAXD profiles for the melt-pressed samples cooled over four different rates together with solution-cast samples annealed at different temperatures (discussed later). In the melt-pressed samples (hollow symbols), note that higher-order maxima ($\sqrt{3}$, $\sqrt{4}$, $\sqrt{7}$, $\sqrt{9}$, and $\sqrt{12}$ relative to that of the first-order diffraction maximum) are observed for the slow-cool and medium-cool samples. This indicates a hexagonally packed cylindrical morphology for these thermal histories. On the other hand, fast-cool and quenched samples show broad higher-order maxima. This indicates that both the order and the average length of PS cylinders increase with grain size.

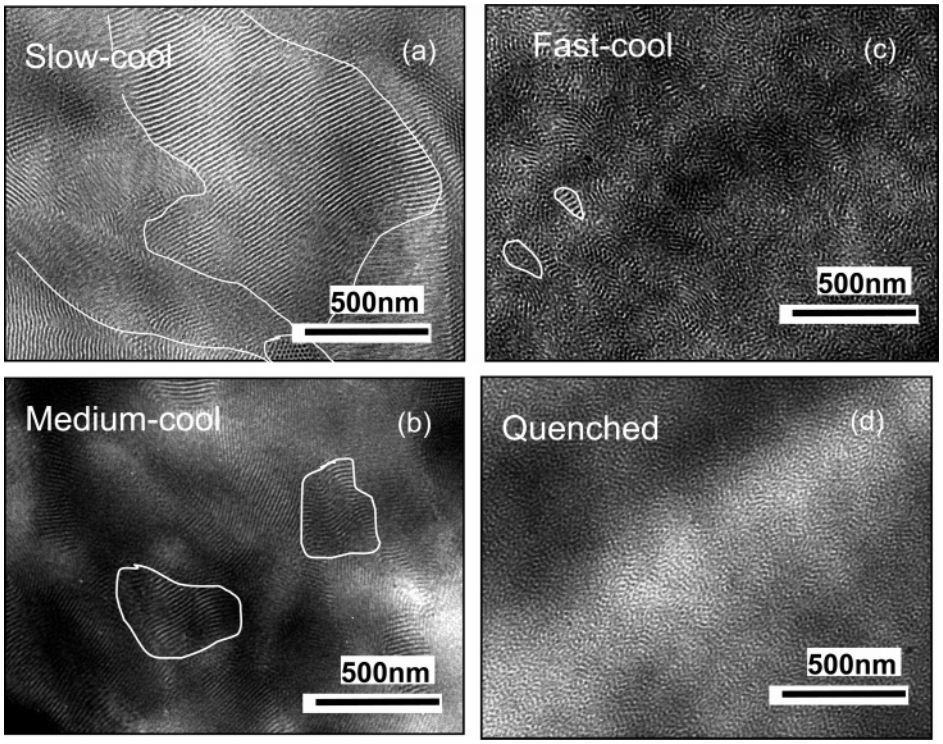

Figure 3. TEM images of melt-processed samples at different cooling rates: (a) slow cool (6−7 h), (b) medium cool (~90 min), (c) fast cool (5−6 min), (d) quenched (less than a minute). The dark phase corresponds to the (PS) cylindrical domains, since ruthenium tetroxide preferentially stains the styrenic phase, while the bright phase corresponds to (PEB) matrix.

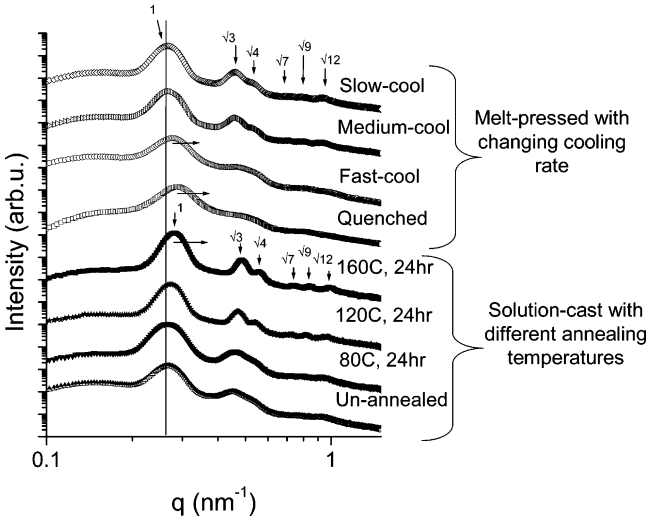

Figure 4. SAXD patterns of the cylindrical system prepared by (i) melt-processing, prepared at different cooling rates (unfilled symbols), and (ii) solution-cast method and then annealed at 80, 120, and 160 °C for 24 h (filled symbols). The profiles have been shifted vertically for clarity.

Monotonic tensile tests were also performed on the melt-pressed samples. Figure 5a shows the stress vs extension ratio plots of these samples, where 6−8 specimens of each sample were tested. It can be noted that there is some variability in the tensile data. Figure 5b shows the representative curves which indicate an average response of Figure 5a. A softer response for the quenched sample (fine grain structure) and a stiffer response for the slow-cool sample (coarse grain structure) are observed. The fast-cool and medium-cool samples show intermediate response. A Mooney−Rivlin[32,33] response was fit to the tensile data and values for the stiffness coefficients were obtained between extension ratios of 2.2 and 3.2. The Mooney−Rivlin equation can be written in the form shown in eq 1

$$\frac{\sigma_{eng}}{\lambda - \frac{1}{\lambda^2}} = 2C_1 + \frac{2C_2}{\lambda^2} \quad (1)$$

where σ_{eng} is the engineering stress, λ is the extension ratio, and C_1 and C_2 are the Mooney−Rivlin stiffness coefficients. The constant C_1 can be associated with the number of mechanically effective cross-links in an ideal network[34] and hence is taken as the rubbery modulus. Table 1 shows the average C_1 values for melt-pressed samples cooled over four different rates together with solution cast and melt-pressed samples annealed at different temperature (discussed later). The elastic modulus (C_1) increases with the order and grain size in the melt-pressed samples. This increase in elastic modulus may be associated with increasing grain size or other changes in the material's microstructure. Additional structural parameters were investigated, and a correlation between *d*-spacing and elastic modulus was also observed (see Table 1). The *d*-spacing in cylindrical block copolymer systems corresponds to the spacing between (100) planes in hexagonally packed PS cylindrical domains. It is a measurable parameter which gives information about the microdomain structure, such as the domain size (diameter) and the interdomain distance. Subtle changes can be observed in the *d*-spacing (see Figure 6, as measured from SAXD patterns in Figure 4) with a decrease in *d*-spacing occurring with increasing cooling rate (the precision of the SAXD instrument is 0.003 nm^{-1}).

3.3. Solution-Cast Films: Effect of Annealing. The TEM micrograph in Figure 7 shows that this block copolymer prepared by solution-casting in toluene phase separates to form PS cylinders embedded in a PEB matrix. Therefore, toluene is not a preferential solvent for this system. SAXD measurement on these systems also confirms the hexagonal packing of PS cylinders in a PEB matrix (see Figure 4).

The microstructural and the mechanical behavior of solution-cast samples are sensitive to parameters such as annealing

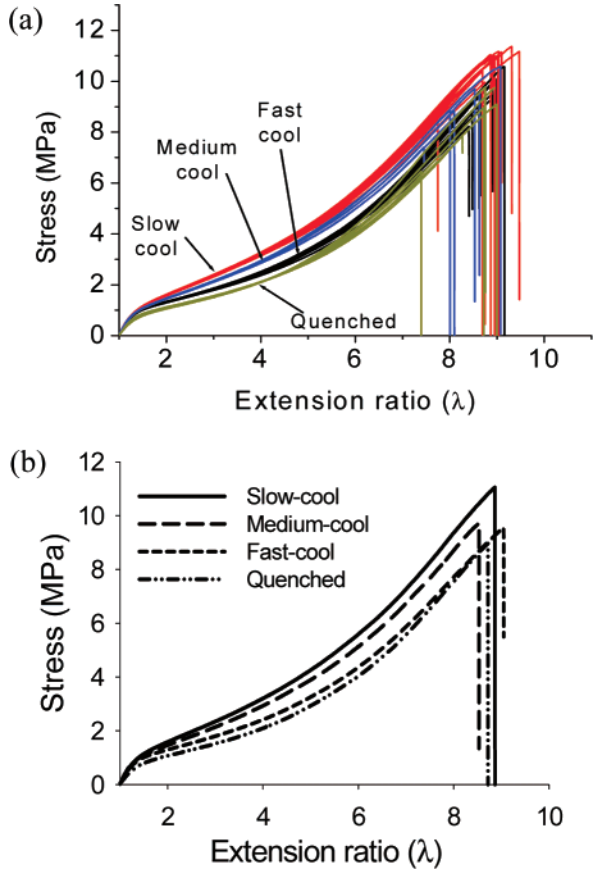

Figure 5. Tensile behavior of melt-pressed samples prepared at different cooling rates: (a) stress vs extension ratio plots of all the samples; (b) representative curves of data in (a).

Table 1. Change in *d*-Spacing Due to Different Sample Preparation Methods and Thermal Histories and Corresponding Changes in Elastic Modulus[a]

treatment	q (nm^{-1})	d (Å)	C_1 (MPa)
melt-pressed at different cooling rates			
melt-pressed slow cool	0.267	235.5	0.335
melt-pressed medium cool	0.27	232.6	0.297
melt-pressed fast cool	0.275	228.3	0.197
melt-pressed quenched	0.287	218.8	0.188
melt-pressed and annealed[a]			
melt-pressed fast cool, 120 °C, 1 h	0.273	229.6	0.2
melt-pressed fast cool, 180 °C, 1 h	0.284	221.3	0.193
melt-pressed fast cool, 120 °C, 24 h	0.270	232.7	0.214
melt-pressed fast cool, 180 °C 24 h	0.280	224.3	0.24
melt-pressed slow cool, 120 °C, 24 h	0.273	229.6	0.293
melt-pressed slow cool, 160 °C, 24 h	0.279	225.4	0.267
solution-cast and annealed[a]			
toluene-cast unannealed	0.263	238.6	0.374
toluene-cast, 80 °C, 24 h	0.267	235.5	0.316
toluene-cast, 120 °C, 24 h	0.274	229.6	0.265
toluene-cast, 160 °C, 24 h	0.280	224.0	0.278

[a] It may be noted that all the annealed samples (solution-cast and melt-pressed and further annealed) were quenched from the high temperature state to 0 °C.

temperature and time. In order to study this effect, solution-cast films were annealed at different temperatures (80, 120, and 160 °C) for 24 h. TEM analysis was done to ascertain any differences in the grain size that may be noted due to different annealing temperatures. Unfortunately, all the TEM images show large grains, and no trends were established. It has been reported[10] that the grain size can only increase with annealing temperature, as the grains will continue to achieve their thermodynamic lower energy state.

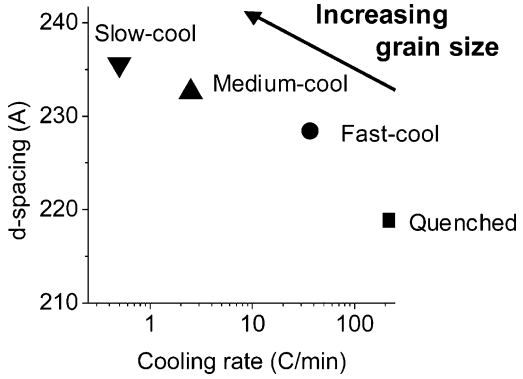

Figure 6. Change in *d*-spacing with cooling rate of the samples prepared by melt-processing. Cooling rate is calculated approximately from the ratio of total change in temperature to total time taken to reach room temperature.

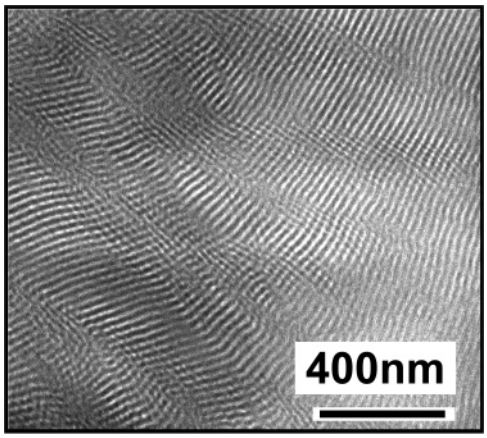

Figure 7. TEM image showing the cylindrical morphology in the SEBS triblock copolymer prepared by solution-cast method.

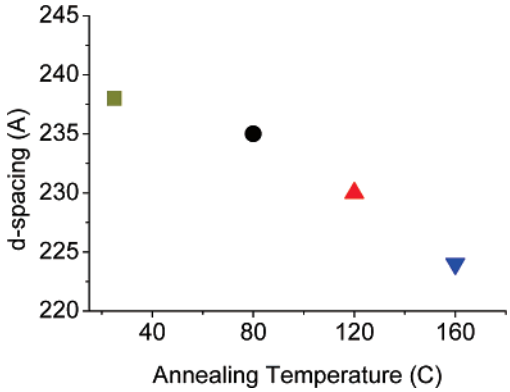

Figure 8. Change in *d*-spacing with annealing temperature of solution-cast samples.

Figure 4 shows the SAXD pattern of solution-cast films annealed at different temperatures (filled symbols). At annealing temperatures 120 and 160 °C (above the T_g of PS block), the SAXD patterns show a higher degree of ordering when compared to the unannealed and 80 °C annealed films. Annealing treatment also affects the *d*-spacing of solution cast films. Note that the *d*-spacing decreases with an increase in annealing temperature (see Figure 8).

Stress vs extension ratio curves for the solution-cast films annealed at 80 and 160 °C along with the unannealed sample are shown in Figure 9a. Note that a higher degree of scatter in the tensile curves can be observed when compared with the melt-pressed systems. In order to statistically evaluate the variability in tensile data illustrated in Figure 9a, a *t*-test was performed

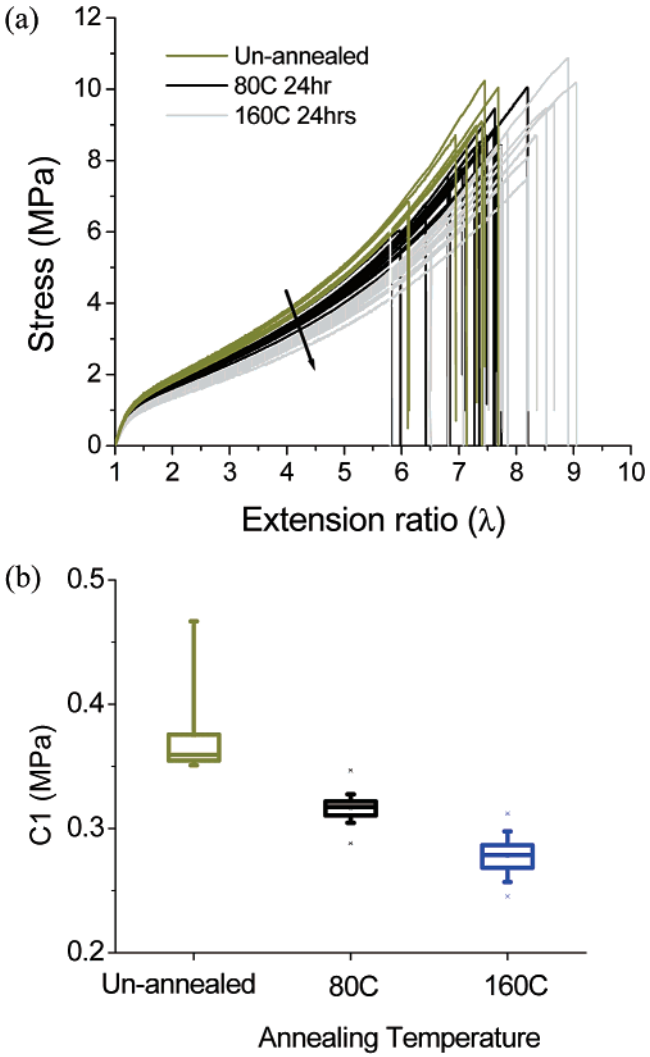

Figure 9. (a) Stress vs extension ratio curves (tensile behavior) for solution-cast films before and after annealing. (b) Average elastic modulus values represented by the Mooney−Rivlin constant C_1 at two different annealing temperatures.

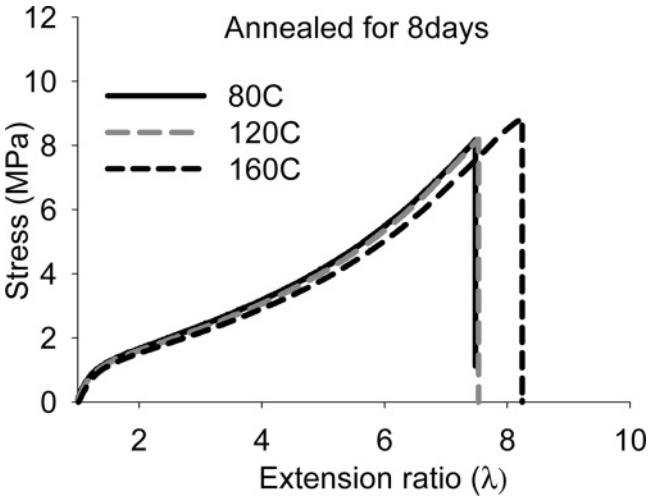

Figure 10. Stress vs extension ratio curves (tensile behavior) of solution-cast films annealed for 8 days.

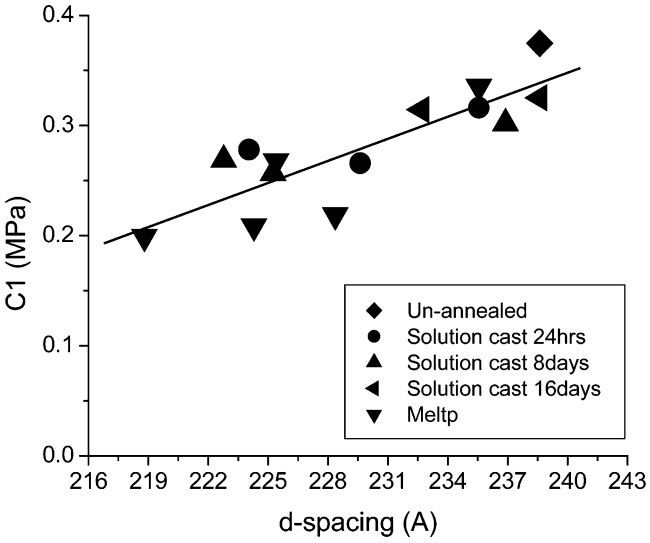

Figure 11. Linear fit showing a correlation of elastic modulus (represented by the Mooney−Rivlin constant C_1) and *d*-spacing.

on selected mechanical parameters. Approximately 17−18 specimens for each temperature and process condition were tested. The *t*-test analysis suggests that there is a significant difference in the elastic modulus of the samples annealed at 80 and 160 °C (i.e., the hypothesis that $C_1^{80°C} = C_1^{160°C}$ can be rejected with a confidence level of 99.9%). Figure 9b shows this difference in the average elastic modulus of the two samples.

The data demonstrate that the material becomes softer with the increase in annealing temperature. The sample annealed at 160 °C, which shows the highest degree of order in SAXD patterns, shows the softest response. These results suggest that as the order increases with annealing temperature, the elastic modulus (C_1) of the system decreases (see Figure 9b).

The effect of annealing at longer times was also investigated. Samples annealed at 80, 120, and 160 °C for 8 days (see Figure 10) show a trend similar to those annealed for shorter times, (i.e., elastic modulus decreased upon annealing at higher temperatures). Also, the sample annealed at 160 °C shows a softer response than those annealed at 80 and 120 °C.

The tensile behavior of these samples (solution-cast films annealed at different temperatures) shows an apparent contradiction. As shown in Figure 9, the elastic modulus decreases with an increase in order and a probable increase in the grain size. This is opposite from the behavior observed in melt-pressed samples where the elastic modulus increases with an increase in order and the grain size. From this apparent contradiction, it may be perceived that the elastic modulus is not affected by the grain size.

However, with regard to *d*-spacing, there does appear to be some correlation with modulus (C_1) for both the melt-pressed and solution-cast samples. This is shown for all cases in Table 1 with the *d*-spacing decreasing with the increase in annealing temperature. This observed correlation between the elastic modulus (C_1) and *d*-spacing, for both the melt-processed and solution-cast films, is shown in Figure 11.

3.4. Effect of Temperature and Cooling Rate on *d*-Spacing. The effect of temperature on the *d*-spacing of block copolymers was first observed by Kawai and co-workers in a series of works.[4,35] They explained that, at a low temperature, the block chains are stretched away from the interface due to a high segregation power (χ), and the segregation power (χ) decreases with increasing temperature ($\chi \sim 1/T$). This results in a thicker or diffused domain boundary and a smaller end-to-end distance of A and B chains at higher temperatures. The smaller end-to-end distance, in turn, results in a smaller domain size and interdomain distance. This decrease in the domain size is easily adjusted by the displacement of chemical junction points along the interface. Hence, the domain size and interdomain distance

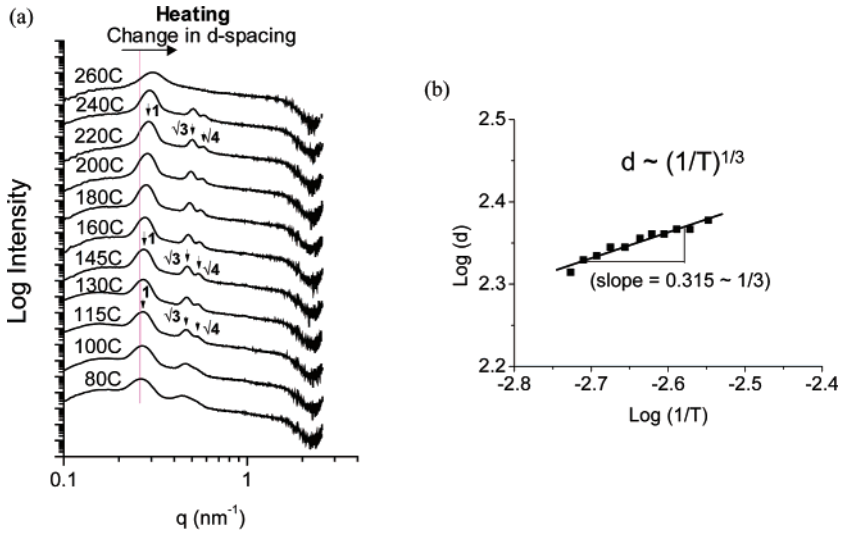

Figure 12. (a) Temperature-resolved SAXD of the solution-cast sample performed at incremental steps of temperature and recorded for 30 min. (b) Plot showing change in *d*-spacing (units in angstroms) with temperature as determined from the position of first-order maxima of the patterns shown in (a).

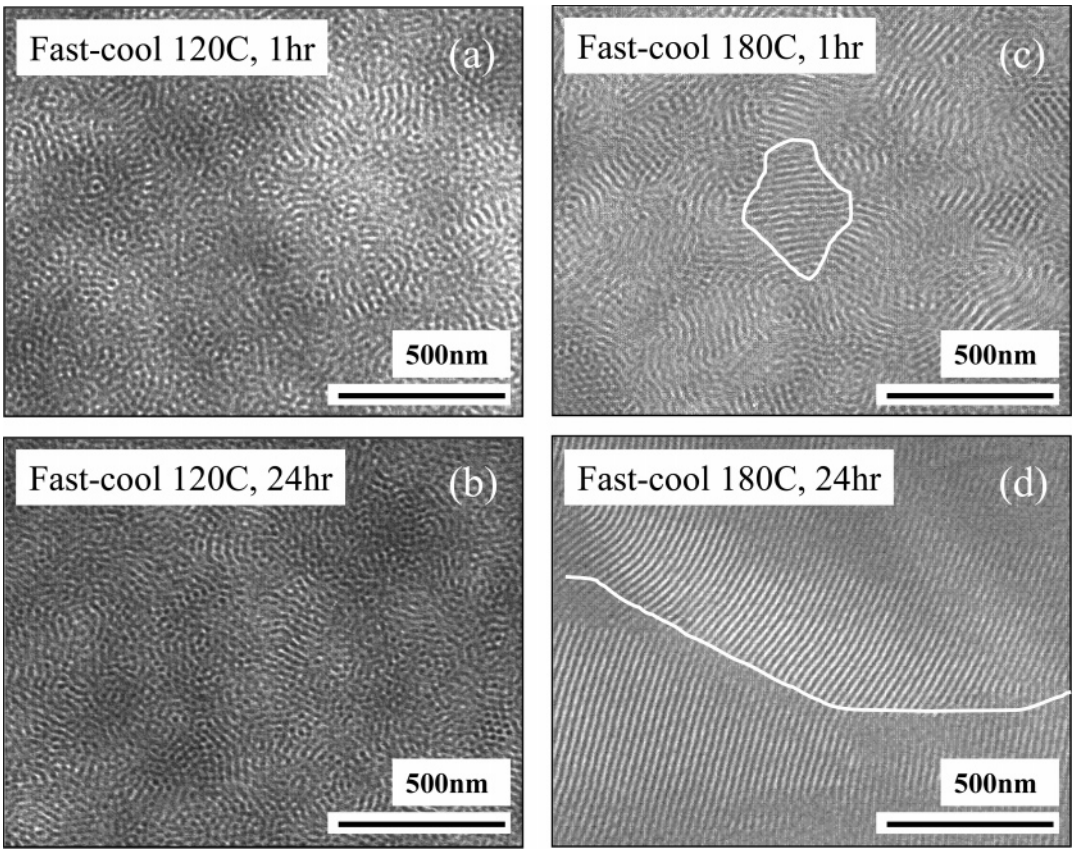

Figure 13. TEM micrographs of fast-cool sample annealed at (a) 120 °C for 1 h, (b) 120 °C for 24 h, (c) 180 °C for 1 h, and (d) 180 °C for 24 h.

are primarily determined by the segregation power of the system (i.e., $d = d(\chi)$). It is observed that the *d*-spacing decreases with increasing temperature as a function of $d \sim (1/T)^{1/3}$.

Temperature-resolved small-angle X-ray diffraction performed on a solution-cast film (Figure 12a) shows that the order increases at temperatures above $T \sim 115$ °C, which is just above the glass transition of poly(styrene). The sample retains its cylindrical morphology up to 240 °C, after which it shows a transition to a disordered state at 260 °C. This rules out the possibility of any order-to-order transition (OOT) in this system. With the increase in temperature, a continuous shift in the position of first-order maxima to higher scattering angles (or scattering wave vector *q*) can be noticed. This shift corresponds to a decrease in *d*-spacing with temperature (Figure 12b) which is associated with the decrease in segregation power (χ), as explained above. This result shows the behavior of *d*-spacing with temperature as $d \sim (1/T)^{\sim 1/3}$, which is in agreement with the findings of Kawai and co-workers.

The changes in *d*-spacing with cooling rate, for melt-pressed samples, can be explained in terms of the kinetics of the process. When fast cooling is employed, the sample is unable to reach its thermodynamic equilibrium state of high segregation power

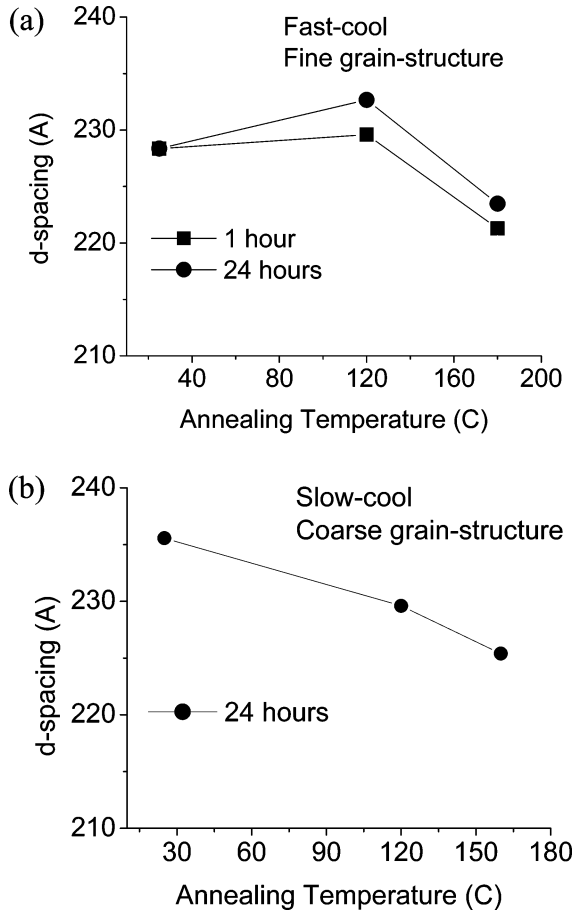

Figure 14. Change in *d*-spacing with annealing temperature and time: (a) fast-cool sample; (b) slow-cool sample.

(χ). This happens because the block chains do not have sufficient time to relax and stretch away from the interface. Hence, the fast-cool and quenched systems at room temperature are far from their thermodynamic equilibrium state, and a structure corresponding to low χ (or smaller *d*-spacing) is kinetically trapped. In a slow-cooling process, the sample has sufficient time to approach its thermodynamic equilibrium state. Therefore, the slow-cool sample has a structure corresponding to high χ or larger *d*-spacing. As shown in Figure 6, the *d*-spacing decreases with increasing cooling rate. Note that the cooling rate is expected to affect the structure up to $T \sim 110$ °C, which corresponds to the glass transition of PS block, below which the system is in a frozen state.

3.5. Correlating Grain Size and/or *d*-Spacing to Elastic Modulus. An additional series of experiments were conducted to further determine whether the mechanical response of these materials correlates only to the *d*-spacing or whether it also depends on the grain size. Unfortunately, the solution-cast samples studied for annealing already had large grains before the thermal treatment. Thus, the grain size did not change significantly upon annealing. In order to study the effect of annealing on grain size, a sample with small grains is required. Therefore, a melt-pressed sample that initially has small grains (i.e., fast-cool sample, see Figure 3c) was annealed at two greatly different temperatures over various times. The fast-cool sample (fine grain structure) was annealed at 120 and 180 °C, for both 1 and 24 h.

The annealing temperatures were selected in order to allow the samples to develop significantly different *d*-spacings. The different annealing times would allow the grain size to increase in both systems. In this way, we can produce smaller grains

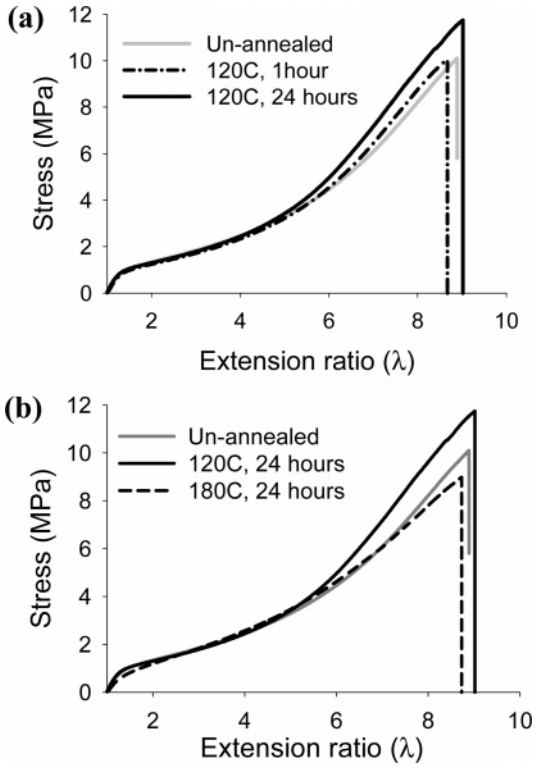

Figure 15. Tensile behavior of fast-cool samples on annealing: (a) at 120 °C for 1 and 24 h; (b) at 120 and 180 °C for 24 h.

with larger *d*-spacings and test their effect on modulus. This together with the prior melt-pressed data will allow us to separate grain size from *d*-spacing. Figure 13 shows the TEM micrographs of these samples. The temperature and time correspond to a different grain size, as the grain size increases with both the annealing temperature and time. At 120 °C, the block copolymer chains lack sufficient mobility and the grain size does not change after annealing for both 1 and 24 h (see Figure 13a,b). However, at 180 °C the chains now attain greater mobility and the grain size increases significantly. A noticeable difference can be seen for the samples annealed at 180 °C for 1and 24 h (see Figure 13c,d).

The annealing treatment also affects their *d*-spacing, as shown in Figure 14a. The *d*-spacing first increases after annealing at 120 °C for both 1 and 24 h and decreases upon annealing at 180 °C. The fast-cool sample, before annealing, is far from its thermodynamic equilibrium state of high segregation power and large *d*-spacing. In other words, a structure corresponding to low segregation power and small *d*-spacing is kinetically trapped. Upon annealing at 120 °C, which is just above the glass transition of PS block, the block chains acquire some mobility, and the sample moves toward its thermodynamic equilibrium state of high segregation power and large *d*-spacing. Hence, the *d*-spacing increases at 120 °C. Note that this chain mobility is not sufficient for the growth of grains. At 180 °C the thermodynamic equilibrium state corresponds to a state of low segregation power (χ), and therefore, the *d*-spacing decreases.

Further, the sample that initially had large grains (slow-cool sample, see Figure 3a) was also annealed at 120 and 160 °C for 24 h. The grain size for this sample is not expected to increase much since it already has large grains. However, the *d*-spacing decreases (see Figure 14b) with temperature ($d \sim T^{-1/3}$), similar to the solution-cast samples. The slow-cool sample, before annealing, is close to its thermodynamic equilibrium of high segregation power (χ) and large *d*-spacing, as

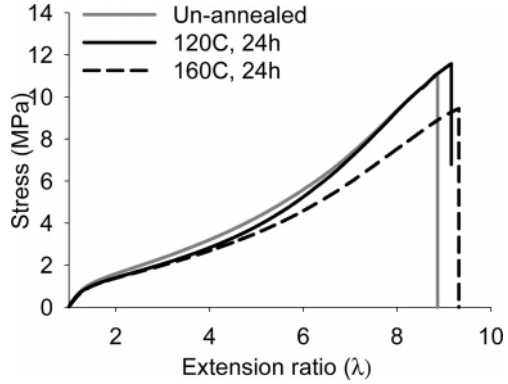

Figure 16. Tensile behavior of slow-cool sample on annealing at 120 and 160 °C for 24 h.

already explained in the previous section. Increasing the temperature results in decreasing segregation power (χ) and hence the *d*-spacing.

These variations in *d*-spacing (Figure 14), due to different annealing temperatures, also affect material's tensile behavior (see Figures 15 and 16). It may be noted that the differences appear only at higher strains in these samples ($6 < \lambda < 8$). Figure 15a shows that the elastic modulus (at higher strains) of the fast-cool sample increases when annealed at 120 °C for 1 h, and it further increases when annealed for 24 h. As previously noted, at 120 °C there is no change in the grain size, but the *d*-spacing increases. This implies that the change in modulus correlates with *d*-spacing as previously observed. Figure 15b shows the effect of temperature when annealed for 24 h. It can be seen that the elastic modulus (at higher strains) increases when annealed at 120 °C and it decreases at 180 °C. Hence, modulus decreases at 180 °C together with the *d*-spacing even though the grain size is increasing. This indicates that *d*-spacing is the primary factor governing the elastic modulus and grain size has a secondary effect. The elastic modulus of the slow-cool sample (already containing large grains) decreases upon annealing at 120 °C, and it further decreases on annealing at 160 °C (see Figure 16). As shown in Figure 14b, the *d*-spacing for this system also decreases with increasing annealing temperature. These results again confirm the correlation between the elastic modulus and the *d*-spacing and not the grain size.

3.6. Cyclic Behavior. Cyclic tests were performed on the melt-pressed samples, where each sample was cycled five times after an initial stretch at various strains. It can be seen that all four samples (slow-cool, medium-cool, fast-cool, and quenched) show a significant Mullins effect[36] (see Figure 17), which is the difference in the first loading curve and subsequent loading and unloading curves. The extent of the Mullins effect increases with a decrease in cooling rate or an increase in *d*-spacing. The quenched sample shows the least Mullins effect, while the slow-cool sample shows the largest Mullins effect. The Mullins effect in cylindrical block copolymers has been shown[21,37] to be associated with a microbuckling of PS cylinders during the first loading cycle, after which the elastomer shows a softer response. Therefore, the extent of Mullins effect should depend on the relative stiffness of an individual cylindrical domain, which is a function of its diameter and modulus. Hence, the extent of Mullins effect increases with the increase in domain diameter (which is directly related to the *d*-spacing). The effect of other structural parameters is not discussed here, as the authors consider this a subject of future studies.

3.7. Single-Grain Systems. Extrusion can impart very high order and orientation in these samples in a single-step process when processed below their ODT.[38] Single-grain samples were prepared below the ODT in the single-screw extruder. Because

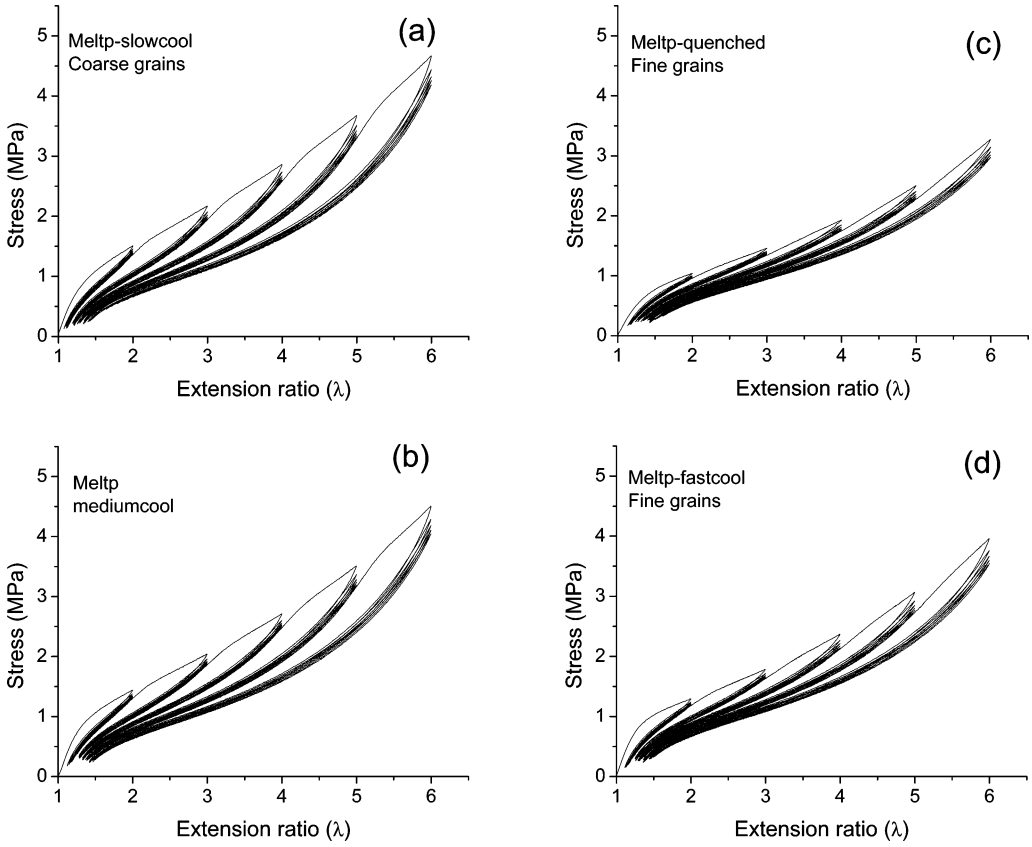

Figure 17. Cyclic behaviors of melt-pressed samples prepared at four different cooling rates: (a) slow cool, (b) medium cool, (c) quenched, and (d) fast cool.

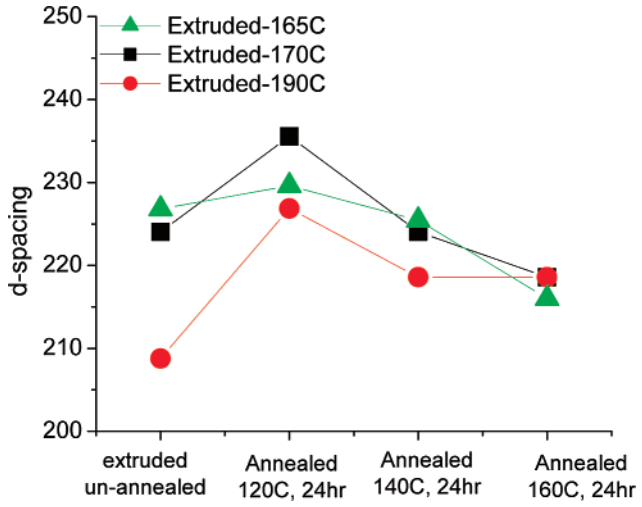

Figure 18. Changes in *d*-spacing of extruded samples on annealing at higher temperatures.

of the shearing effects inside the screw, the cylindrical domains orient along the screw axis. The samples prepared at different temperatures showed differences in their *d*-spacing. The *d*-spacing decreases as the temperature of the extruder increases. As the sample, at a high temperature, comes out of the extruder, it cools quickly in air, and hence a low χ-like structure is kinetically trapped. Upon annealing these samples at higher temperatures for 24 h, the *d*-spacing first increases at 120 °C and then decreases at higher annealing temperatures (see Figure 18). This behavior is similar to what we have already seen for the fast-cool sample (Figure 14a). This indicates that single-grain systems also exhibit changes in the *d*-spacing due to different process conditions and thermal treatments. A change in the mechanical behavior of these single-grain systems due to changes in *d*-spacing is a subject of future consideration.

4. Conclusions

In this paper, we present a correlation between a measurable structural parameter and the mechanical response of commercially relevant SEBS triblock copolymers containing cylindrical morphology. We show that a linear correlation exists between the elastic modulus (C_1) and *d*-spacing. This correlation exists over a broad range of thermal and process conditions including effects from annealing and cooling. The *d*-spacing, which is associated with the domain size, decreases with an increase in the annealing temperature as the system evolves to a thermodynamic state. The *d*-spacing also decreases with an increase in the cooling rate, and the behavior is explained in terms of the kinetics of the process. The extent of Mullins effect also increases with the *d*-spacing.

Additional studies were also performed to isolate what effect, if any, the grain size has on the elastic modulus. It was shown that the grain size has a secondary effect on the elastomer's response. The grain size was shown to increase with a corresponding decrease in cooling rate on melt-pressed samples. It was also shown that the grain size increased with annealing temperature. However, in both cases the elastic modulus was shown to be relatively insensitive to the changes in grain size.

Acknowledgment. The authors thank the Center for University of Massachusetts and Industry Research on Polymers (CUMIRP) Cluster-M and Kraton Polymers LLC for their support and the National Science Foundation Materials Research Science and Engineering Center for their financial support.

References and Notes

(1) Leibler, L. *Macromolecules* **1980**, *13*, 1602−1617.
(2) Ohta, T.; Kawasaki, K. *Macromolecules* **1986**, *19*, 2621−2632.
(3) Thomas, E. L.; Lescanec, R. L.; Frank, F. C.; Higgins, J. S.; Klug, A.; Hamley, I. *Philos. Trans.: Phys. Sci. Eng.* **1994**, *348*, 149−166.
(4) Shibayama, M.; Hashimoto, T.; Kawai, H. *Macromolecules* **1983**, *16*, 16−28.
(5) Honeker, C. C.; Thomas, E. L. *Chem. Mater.* **1996**, *8*, 1702−1714.
(6) Lach, R.; Weidisch, R.; Knoll, K. *J. Polym. Sci., Part B: Polym. Phys.* **2005**, *43*, 429−438.
(7) Lach, R.; Weidisch, R.; Janke, A.; Knoll, K. *Macromol. Rapid Commun.* **2004**, *25*, 2019−2024.
(8) Zhu, Y.; Weidisch, R.; Gido, S. P.; Velis, G.; Hadjichristidis, N. *Macromolecules* **2002**, *35*, 5903−5909.
(9) Pakula, T.; Saijo, K.; .; Kawai, H.; Hashimoto, T. *Macromolecules* **1985**, *18*, 1294−1302.
(10) Yamaguchi, D.; Hashimoto, T.; Vaidya, N. Y.; Han, C. D. *Macromolecules* **1999**, *32*, 7696−7699.
(11) Kim, W. G.; Chang, M. Y.; Garetz, B. A.; Newstein, M. C.; Balsara, N. P.; Lee, J. H.; Hahn, H.; Patel, S. S. *J. Chem. Phys.* **2001**, *114*, 10196−10211.
(12) Gido, S. P.; Gunther, J.; Thomas, E. L. *Macromolecules* **1993**, *26*, 4606−4520.
(13) Gido, S. P.; Thomas, E. L. *Macromolecules* **1994**, *27*, 849−861.
(14) Gido, S. P.; Thomas, E. L. *Macromolecules* **1994**, *27*, 6137−6144.
(15) Balsara, N. P.; Garetz, B. A.; Dai, H. J. *Macromolecules* **1992**, *25*, 6072−6074.
(16) Chang, M. Y.; Abuzaina, F. M.; Kim, W. G.; Gupton, J. P.; Garetz, B. A.; Newstein, M. C.; Balsara, N. P.; Yang, L.; Gido, S. P.; Cohen, R. E.; Boontongkong, Y.; Bellare, A. *Macromolecules* **2002**, *35*, 4437−4447.
(17) Abuzaina, F. M.; Garetz, B. A.; Mody, J. U.; Newstein, M. C.; Balsara, N. P. *Macromolecules* **2004**, *37*, 4185−4195.
(18) Garetz, B. A.; Newstein, M. C.; Dai, H. J.; Jonnalagadda, S. V.; Balsara, N. P. *Macromolecules* **1993**, *26*, 3151−3155.
(19) Myers, R. T.; Cohen, R. E. *Macromolecules* **1999**, *32*, 2706−2711.
(20) Beyer, F. L.; Gido, S. P.; Buschl, C.; Iatrou, H.; Uhrig, D.; Mays, J. W.; Chang, M. Y.; Garetz, B. A.; Balsara, N. P.; Tan, N. B.; Hadjichristidis, N. *Macromolecules* **2000**, *33*, 2039−2048.
(21) Indukuri, K. K. Ph.D. Thesis, In *Polymer Science and Engineering*; University of Massachusetts, Amherst: Amherst, MA, 2005.
(22) Choi, S.; Vaidya, N. Y.; Han, C. D.; Sota, N.; Hashimoto, T. *Macromolecules* **2003**, *36*, 7707−7720.
(23) Perahia, D.; Vacca, G.; Patel, S. S.; Dai, H. J.; Balsara, N. P. *Macromolecules* **1994**, *27*, 7645−7649.
(24) Sakurai, S.; Umeda, H.; Yoshida, A.; Nomura, S. *Macromolecules* **1997**, *30*, 7614−7617.
(25) Kimishima, K.; Jinnai, H.; Hashimoto, T. *Macromolecules* **1999**, *32*, 2585−2596.
(26) Andre, D.; Bernard, G. *Makromol. Chem.* **1972**, *156*, 81−115.
(27) Mamodia, M.; Lesser, A. J. SPE Annual Technical Conference, Cincinnati, OH, 2007.
(28) Lyon, R. E.; Raboin, P. J. *J. Therm. Anal. Calorim.* **1995**, *44*, 777−793.
(29) Indukuri, K. K.; Lesser, A. J. *Polymer* **2005**, *46*, 7218−7229.
(30) Lyon, R. E. Ph.D. Thesis, In *Polymer Science and Engineering*; University of Massachusetts, Amherst: Amherst, MA, 1984.
(31) Lyon, R. E.; Farris, R. J. *Polym. Sci. Eng.* **1984**, *25*, 908−914.
(32) Rivlin, R. S. *Philos. Trans. R. Soc. London, Ser. A* **1948**, *241*, 379−397.
(33) Mooney, M. *J. Appl. Phys.* **1940**, *11*, 582−592.
(34) Spathis, G. D. *J. Appl. Polym. Sci.* **1991**, *43*, 613−620.
(35) Hashimoto, T.; Shibayama, M.; Kawai, H. *Macromolecules* **1983**, *16*, 1093−1101.
(36) Mullins, L. *Rubber Chem. Technol.* **1969**, *42*, 339−361.
(37) Indukuri, K. K.; Atkins, E. T.; Lesser, A. J. MRS Spring Meeting, San Francisco, 2005.
(38) Indukuri, K. K.; Atkins, E. T.; Lesser, A. J. ANTEC 2005 Meeting, Boston, MA, 2005.

MA070006+